Universität Karlsruhe (TH)
Forschungsuniversität • gegründet 1825

Institut für Mechanik

Measures to judge the sensitivity of thin-wall shells concerning stability under different loading conditions

Eduard Ewert, Karl Schweizerhof, Peter Vielsack
Universität Karlsruhe, Institut für Mechanik

2005

Institut für Mechanik
Kaiserstr. 12, Geb. 20.30
76128 Karlsruhe
Tel.: +49 (0) 721/ 608-2071
Fax: +49 (0) 721/ 608-7990
E-Mail: ifm@uni-karlsruhe.de
www.ifm.uni-karlsruhe.de

Eduard Ewert · Karl Schweizerhof · Peter Vielsack

Measures to judge the sensitivity of thin-walled shells concerning stability under different loading conditions

Abstract In standard stability investigations of structures applying the finite element method usually the bifurcation and snap-through points – so-called stability points – are detected. However, for practical design purposes not only the stable state of equilibrium itself is significant but also the robustness of the state against finite perturbation in contrast to infinitesimal perturbation. The sensitivity measure, which quantifies this robustness, can be investigated by introducing perturbations at certain load levels and considering the perturbed motion. Some sensitivity studies are performed for simple stability problems as well as for realistic structures (cylindrical shells) under different loading conditions. Further scalar parameters based on Liapunov Characteristic Exponents are developed to allow a better judgment of the motion after introducing perturbation and a more efficient analysis of the complex response (see Ewert/Schweizerhof [7]).

Keywords structural stability · sensitivity · transient analysis · shell structures

1 Introduction

Stability investigations with Finite Elements are currently performed assuming a static behaviour for the pre- and post-buckling region. Most algorithms follow a somehow standard procedure: a so-called linear eigenvalue analysis is performed assuming a fully elastic buckling process. For this purpose the tangent stiffness matrix is mostly separated in constant and linear or nonlinear terms; different formulations for the terms are possible (see Ramm [13], Brendel [3], Helnwein [9]). Depending on the amount of the nonlinearity

Karl Schweizerhof
Institut fuer Mechanik, University of Karlsruhe, 76131 Karlsruhe, Germany
Tel.: +49-(0)721-608-2070
Fax: +49-(0)721-608-7990
E-mail: karl.schweizerhof@ifm.uni-karlsruhe.de

the predictions of the so-called stability points, bifurcation or snap-through points, are more or less accurate. The more cumbersome alternative is the computation of a full load-deflection path monitoring the determinant and the eigenvalues of the tangent stiffness matrix. The accompanying eigenvalue analysis have the advantage that the eigenmodes give e.g. further information on possible measures to avoid buckling (see Brendel [3]). More sophisticated techniques allow the direct computation of buckling loads (see Wriggers et al. [22]). In the present contribution the nonlinear computation monitoring some lower eigenvalues is used to determine singular points of shells, bifurcation or snap through points.

The post-buckling behavior resp. the post-buckling region of the nonlinear load deflection path can be investigated neglecting dynamics with the well known arc-length method and path-switching procedures. Other solution techniques based an the asymptotic expansion allow a fairly efficient computation of post-buckling branches (see Baguet et al. [1]). For rather simple FE models with small numbers of degrees of freedom these procedures provide satisfactory results. However, for more complex structures such as shells the computation of post-buckling paths assuming static behaviour becomes rather difficult and questionable, in particular concerning the lowest post-buckling load, which is used to judge safety against stability failure. This is mostly due to badly conditioned matrices involved in the analysis then and due to the fact that a sequence of bifurcation points occur mostly in the post-buckling region and thus a sufficient analysis of this region appears impossible even with the most sofisticated numerical instruments available today.

Many limits of the static approach mentioned above are due to the fact that buckling is in reality a dynamic process. Thus, many static states of equilibrium in the post-buckling region are not only difficult to compute but also of no practical relevance. Thus, we suggest to model the complete loading and deformation behaviour by a time-dependent process. The major advantage of a purely transient analysis is the complete simulation of the buckling process as it happens in reality. This is possible with a moderate numerical effort, since the matrices used in the solution are usually better conditioned compared to pure static analysis, e.g. applying a Newmark type algorithm within the current contribution. This procedure is used to compute the post-buckling loads of a cylinder under axial compression. For a cylinder under external pressure resp. vacuum loading a post-buckling load is computed using an explicit time integration method considering the loading and different unloading processes.

The transient analyses can also be used in the investigation of sensitivity – not by varying the imperfections but by varying the initial conditions. The idea of sensitivity investigations in a static sense known as *the perturbation energy method* is proposed by Kröplin [11] and the following works of Tranel [21] and Spohr [20]. This method is based on a purely static approach, in which a perturbation vector is applied to structures at a defined load level. The static perturbation vector has to be scaled, until the next unstable state of equilibrium is obtained, which may be a problem.

In order to compute a sensitivity measure, in the present contribution, *ki-*

netic perturbations are applied to structures at a given load level followed by a transient analysis. The range and the shape of the perturbations is varied, such that conclusions can be drawn for practical purposes and design rules.

2 Static vs. transient analysis

2.1 Static criteria

In nonlinear finite element analysis the system of equations

$$\boldsymbol{r}(\boldsymbol{u}) - \lambda \boldsymbol{p} = \boldsymbol{0}. \tag{1}$$

must be solved to compute states of equilibrium Herein $\boldsymbol{r}$ denotes the vector of internal forces, $\boldsymbol{p}$ the load vector and λ the load multiplier. For a Newton type solution the linearization of (1) leads to

$$\boldsymbol{K}_T(\boldsymbol{u}_i)\Delta\boldsymbol{u}_{i+1} = \lambda\boldsymbol{p} - \boldsymbol{r}(\boldsymbol{u}_i) \tag{2}$$

with the update of displacements

$$\boldsymbol{u}_{i+1} = \boldsymbol{u}_i + \Delta\boldsymbol{u}_{i+1}. \tag{3}$$

Herein $\boldsymbol{K}_T$ denotes the tangent stiffness matrix dependent on the current displacement state and $\Delta\boldsymbol{u}_{i+1}$ is the vector of the displacement increments for the next iteration step. Within the incremental iterative solution process involving an update of the displacement vector the iterations are performed until a certain tolerance is met and convergence is achieved. The tangent stiffness matrix $\boldsymbol{K}_T$, which is obtained by linearization, can be used in stability investigations of converged states of equilibrium.
It is well known, that for conservative systems which are considered here a state of equilibrium is stable, if $\boldsymbol{K}_T$ is positive definite, i.e. all eigenvalues μ from the standard eigenvalue problem

$$(\boldsymbol{K}_T - \mu\boldsymbol{I})\,\boldsymbol{\Psi} = \boldsymbol{0} \tag{4}$$

are greater than zero. Another commonly used stability criterion is based on the determinant of $\boldsymbol{K}_T$. As the transition from stable to unstable equilibrium states is characterized by zero eigenvalues $\mu = 0$, the characteristic equation of (4) gets

$$det(\boldsymbol{K}_T) = 0. \tag{5}$$

Using these criteria singular points can be determined in combination with bisection procedures. Another tool to determine singular points is an accompanying eigenvalue analysis (see e.g. Brendel [3]). Herein, the tangential matrix at a load level of λ_0 with $\boldsymbol{u}_0$ is expanded into a series with the parameter Λ. For the investigated problems this parameter Λ represents then an additional load multiplier. Truncating the expansion of $\boldsymbol{K}_T$ after the linear term the equation (5) leads to

$$det\,(\boldsymbol{K}_T) = det(\boldsymbol{K}_{T0}|_{\lambda_0} + \Lambda\boldsymbol{K}_{T1}|_{\lambda_0}) = 0 \tag{6}$$

with the corresponding eigenvalue problem

$$(\boldsymbol{K}_{T0}|_{\lambda_0} + \Lambda\boldsymbol{K}_{T1}|_{\lambda_0})\boldsymbol{\phi} = \boldsymbol{0}. \tag{7}$$

$\boldsymbol{K}_{T0}$ represents the tangential stiffness matrix at the load level λ_0 and $\boldsymbol{K}_{T1}$ represents the first derivative of $\boldsymbol{K}_T$ with respect to λ. For the load level below the critical level, a linear approximation for the critical load is obtained as

$$\lambda_{cr} = \lambda_0 + \Lambda. \tag{8}$$

The procedure is known as linear buckling analysis, if the matrices $\boldsymbol{K}_{T0}$ and $\boldsymbol{K}_{T1}$ are computed for the unloaded structure, i.e. at $\lambda_0 = 0$. Solving the equation (7) at varying load levels within a nonlinear computation, in which the load is applied incrementally and equation (2) is solved in each load step, we get a so-called accompanying buckling analysis.

A procedure directed towards the computation of the bifurcation points resulting in an extended system of equations is given in Wriggers et al. [22]. There the condition of zero eigenvalues is introduced into (4) resulting in

$$\boldsymbol{K}_T \boldsymbol{\Psi} = \boldsymbol{0} \tag{9}$$

and included as an additional constraint into the non-linear solution procedure. Then, taking into account also a normalizing constraint, the singular point can be estimated with rather high accuracy. If the singular point is a bifurcation point, all branching paths may be of interest. In principle it is possible to compute them, adding scaled eigenmodes $\zeta\boldsymbol{\Psi}$ to the displacements with small ζ, see Wagner at al. [23]. However, it is an open question, whether this leads to any further information, as a purely static view does not take into account the real physical behaviour.

2.2 Transient analysis

Performing a transient analysis step by step procedures are applied in the context of nonlinear problems. Then the equation of motion (10) has to be solved for each time step $n+1$ ($t_{n+1} = t_n + \Delta t$). This can be done e.g. according to a Newmark type scheme using an interpolation of displacements (11) and velocities (12).

$$\boldsymbol{M}\ddot{\boldsymbol{u}} + \boldsymbol{C}\dot{\boldsymbol{u}} + \boldsymbol{r}(\boldsymbol{u}) - \lambda\boldsymbol{p} = \boldsymbol{0} \tag{10}$$

$$\boldsymbol{u}_{n+1} = \boldsymbol{u}_n + \Delta t\dot{\boldsymbol{u}}_n + \Delta t^2 \left[\left(\frac{1}{2} - \beta \right) \ddot{\boldsymbol{u}}_n + \beta\ddot{\boldsymbol{u}}_{n+1} \right] \tag{11}$$

$$\dot{\boldsymbol{u}}_{n+1} = \dot{\boldsymbol{u}}_n + \Delta t \left[(1-\gamma)\, \ddot{\boldsymbol{u}}_n + \gamma\ddot{\boldsymbol{u}}_{n+1} \right] \tag{12}$$

In addition for the nonlinear case equation (10) must be linearized in a similar way as equation (1) when combined with a Newton type scheme. With (11) and (12) the linearization of (10) leads to the following equation

$$\tilde{\boldsymbol{K}} \Delta\boldsymbol{u}_{n+1}^{i+1} = \lambda\boldsymbol{p} - \left(\boldsymbol{r}(\boldsymbol{u}_{n+1}^{i}) + \boldsymbol{C}\dot{\boldsymbol{u}}_{n+1}^{i} + \boldsymbol{M}\ddot{\boldsymbol{u}}_{n+1}^{i} \right). \tag{13}$$

with the so-called generalized tangent matrix $\tilde{\boldsymbol{K}}$

$$\tilde{\boldsymbol{K}} = \frac{1}{\Delta t^2 \beta}\boldsymbol{M} + \frac{\gamma}{\Delta t \beta}\boldsymbol{C} + \boldsymbol{K}_T(\boldsymbol{u}_{n+1}^{i}). \tag{14}$$

Equation (13) has to be solved in each time step $n+1$ iteratively using the displacement update (3) until convergence is achieved. Then we proceed to the next time-step. Concerning stability no information can be gained from the tangent matrix.

2.3 Discussion

For structures with rather linear behaviour in the pre-buckling region singular points can be computed with rather good accuracy and little computational effort using the linearized eigenvalue problem (7) with an expansion at $\lambda_0 = 0$. The critical load is then given by $\lambda_{cr} = \Lambda$. Investigating structures with nonlinear pre-buckling behaviour a nonlinear analysis has to be performed using e.g. the bisection procedure for the constraint (5). In this case at the critical point itself Λ is identical to zero, i.e. the critical load is $\lambda_{cr} = \lambda_0$. For realistic structure with fine FE meshes a rather high numerical effort is needed for this investigation. The procedure with the extended system of equations (Wriggers [22]) is then more efficient. However, the latter is less reliable for general structures, because convergence to the lowest singular point is not ensured. For structures with many singular points, e.g. imperfect cylinders under axial compression, this method suffers often from convergence problems and often some singular points may be bypassed.
Even if in this static analysis the nonlinear load-deflection path can be computed up to the first bifurcation resp. limit point and path switching is successfully completed, considerable effort is necessary as further bifurcation and limit points rather frequently occur on the post-buckling paths. Then each path has to be followed to achieve a full overview over the possible post-buckling equilibrium paths, where for practical purposes the focus is on the post-buckling minimum. This becomes a rather unrealistic task for shell structures with sufficiently fine meshes and many closely spaced bifurcation points. Furthermore equilibrium paths may exist, which have no connection to the primary path and which cannot be reached using static analyses.
For transient analyses no such simple stability criteria as in the static case exist. In principle all possible perturbations in initial conditions have to be considered, in order to investigate the stability of the obtained motion. Beyond that, the buckling behaviour of shells can be computed using transient analyses avoiding the convergence problems occurring in static analyses, as the condition number of $\tilde{\boldsymbol{K}}$ is in general considerably smaller than the condition number of $\boldsymbol{K}_T$, as a result of positive definite mass matrices $\boldsymbol{M}$ and mostly rather small time steps Δt in equation (14). Thus the transient behaviour of shell structures including the real physical buckling behaviour can be easily computed. Several ways are suggested in the literature e.g. Riks, Rankin and Brogan [14] proposal to compute the pre-buckling region in a standard fashion using static analyses, followed then by a transient analysis for the buckling and post-buckling process. Within such a procedure the point in time of the initiation of the buckling process has to be determined, which is fairly difficult. Thus, it has proven to be far more convenient to use a transient analysis with standard time integration schemes even for the static respectively quasi-static part of the process.

3 Sensitivity analysis – definition and procedure.

For systems with more than one state of equilibrium at a defined load level a finite perturbation, e.g. by an initial velocity, can transfer the mechanical sys-

tem out of the basin of attraction of the original stable state of equilibrium. Then the structure can either move to another stable state of equilibrium or perform an unbounded motion. In order to quantify the size of the perturbation in combination with the applied static loading a sensitivity measure is defined as the reciprocal value of the minimum perturbation energy, necessary for this transfer. This energy is equal to the difference $\Delta\Pi$ of the potential to the next unstable state of equilibrium according to a proposal of Vielsack [24] (see Fig. 1).

$$S = \frac{1}{\Delta\Pi} = \frac{1}{W_{p,min}} \tag{15}$$

From this definition it follows that a mechanical system is stable and insensitive against any perturbation for $S = 0$, i.e. only one state of equilibrium exists at this load level. If $S > 0$ the structure is sensitive and the sensitivity is increasing with e.g. a further reduction of the minimum perturbation energy, i.e. several states of equilibrium exist at this load level. An unstable system is obtained for $S \to \infty$, e.g. at a so-called stability point.
To compute the defined sensitivity measure the procedure described in the following is applied. First static nonlinear analysis usually under a given external loading $\lambda \boldsymbol{p}$ is performed in order to reach the state of equilibrium to be analyzed. For this purpose the linearized equation of equilibrium (2) is solved iteratively to obtain finally the displacement vector $\boldsymbol{u}_0$ for a given load level λ_0.
In the next step a *perturbation* is introduced by setting a velocity pattern as initial conditions $\dot{\boldsymbol{u}}_0$. Then the perturbation energy can be computed as

$$W_p = W_{kin} = \frac{1}{2}\dot{\boldsymbol{u}}_0^T \boldsymbol{M} \dot{\boldsymbol{u}}_0 \tag{16}$$

with $\boldsymbol{M}$ as mass matrix. After introducing the perturbation *the perturbed motion* must be computed with the initial conditions $\boldsymbol{u}_0$ and $\dot{\boldsymbol{u}}_0$. Within this step the previously applied loading $\lambda_0 \boldsymbol{p}$ is kept constant. The perturbed motion is obtained solving the equation of motion (10) e.g. using a Newmark type scheme, see section 2.2. The perturbed motion has now to be checked, whether the initial basin of attraction is left or not. In the latter case the structure vibrates around the investigated stable state of equilibrium $(\lambda_0 \boldsymbol{p}, \boldsymbol{u}_0)$ see Fig. 2. Then a next analysis step follows with either increased or decreased perturbation energy respectively. Following this procedure the minimum perturbation energy, which is equal to the minimum kinetic energy, can be determined iteratively with a defined accuracy. Then the sensitivity can be computed via

$$S = \frac{1}{W_{kin,min}}. \tag{17}$$

This value could be made dimensionless using e.g. the internal energy at the investigated stable state of equilibrium. The main questions are:

- How to judge the perturbed motion efficiently and cast it into an algorithm ("automatically")?
- Which pattern of the perturbation vector $\dot{\boldsymbol{u}}_0$ leads to the minimum perturbation energy?

These questions are discussed in the following.

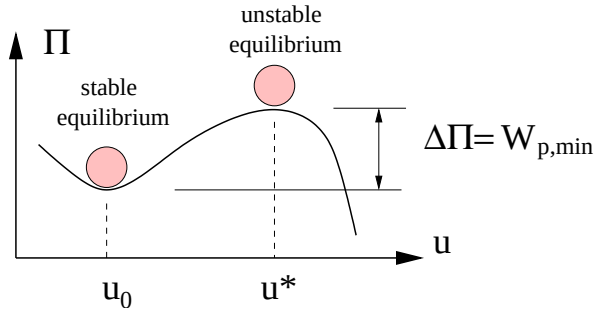

Fig. 1 Definition of the perturbation energy for simple ....

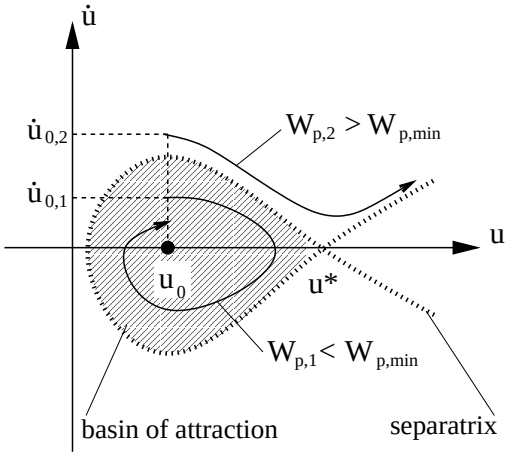

Fig. 2 Typical phase-portraits for the motions of the example in Fig. 1 for different perturbation energies at a defined load level $\lambda_0 \boldsymbol{p}$.

4 Judgment of the perturbed motion.

In the case of small perturbation energies, smaller than $W_{p,min}$, the structure vibrates around the original state of equilibrium $\boldsymbol{u}_0$. In order to achieve a distinct motion towards the attractor, see Fig.2, some damping has to be incorporated into the system. This case represents then a "stable situation" in terms of the sensitivity investigations. For higher perturbation energies than $W_{p,min}$ the structure moves to another stable state of equilibrium or performs an unbounded motion, which indicates a so-called "unstable situation". For rational judgment of the perturbed motions an indicator is needed, that allows an algorithmic and then automatic and efficient decision, whether a critical perturbation energy is obtained. From the Liapunov Characteristic Exponent an indicator can be derived, which allows such a decision.
The Liapunov Characteristic Exponent (LCE) allows to distinguish between stable and unstable motions and is defined as

$$\mathcal{L} = \lim_{t \to \infty} (\mathcal{L}(t)) \tag{18}$$

with

$$\mathcal{L}(t) = \lim_{\boldsymbol{\delta}_0 \to 0} \left(\frac{1}{t} \ln \frac{||\boldsymbol{\delta}(t)||}{||\boldsymbol{\delta}_0||} \right). \tag{19}$$

$\mathcal{L}$ denotes the LCE, $\boldsymbol{\delta}_0$ an initial perturbation and $\boldsymbol{\delta}(t)$ the perturbation at the time point t. $||\dots||$ represents some norm of the perturbation vector. In this case the perturbation vector is defined as the "distance" between the reference motion $\boldsymbol{a}_r$ and some perturbed motion $\boldsymbol{a}_p$ in phase space

$$||\boldsymbol{\delta}_0|| = || \left(\tilde{\boldsymbol{u}}(t=0), \dot{\tilde{\boldsymbol{u}}}(t=0) \right) || \tag{20}$$

and

$$||\boldsymbol{\delta}(t)|| = || \left(\tilde{\boldsymbol{u}}(t), \dot{\tilde{\boldsymbol{u}}}(t) \right) || \tag{21}$$

with

$$\tilde{\boldsymbol{u}} = \boldsymbol{u}_r - \boldsymbol{u}_p \quad \text{and} \quad \dot{\tilde{\boldsymbol{u}}} = \dot{\boldsymbol{u}}_r - \dot{\boldsymbol{u}}_p \tag{22}$$

When $\boldsymbol{a}_p$ converges asymptotically to $\boldsymbol{a}_r$ the LCE $\mathcal{L}$ gets negative, see Fig. 3. The LCE becomes zero, when $\boldsymbol{\delta}$ remains constant, and it becomes positive, when the trajectories diverge, e.g. in the case of chaotic motion.
The very important fact is, that $\mathcal{L}$ remains constant independent of the chosen perturbation and of the chosen reference motion, if both motions start in the "same region" (see Benettin et al. [2]). That means, that e.g. for the case of asymptotic convergence the LCE remains constant for all perturbed motions, which converge towards the defined reference motion, independent of the value of initial perturbation $\boldsymbol{\delta}_0$. Therefore in equation (19) the limitation concerning $\boldsymbol{\delta}_0 \to 0$ can be neglected. Additionally taking into account equations (20) and (21) we get

$$\mathcal{L}(t) = \frac{1}{t} \ln \frac{|| \left(\tilde{\boldsymbol{u}}(t), \dot{\tilde{\boldsymbol{u}}}(t) \right) ||}{|| \left(\tilde{\boldsymbol{u}}_0, \dot{\tilde{\boldsymbol{u}}}_0 \right) ||}. \tag{23}$$

As already mentioned, the main objective is to get an indicator, which separates the motion approaching the original stable state of equilibrium from the other possible motions: a motion to a neighboring stable state of equilibrium or an unbounded motion. All three motions are actually stable in terms of the original definition of LCE, because infinitesimal perturbations $\boldsymbol{\delta}_0 \to 0$ lead to bounded deviations from the investigated motion; the special case of the motion on the separatrix can be neglected because of the included damping, see Fig. 2. Taking into account the constraint of Benettin [2] for the value of the perturbation vector $\boldsymbol{\delta}_0$ we can state, that only the exponents for the "stable situation" in terms of sensitivity analysis represent the Liapunov Characteristic Exponents, as the motions in this case start in the "same region". Despite the fact that the exponents for the "unstable situation" do not represent the LCE in terms of its original definition, they are called LCE in this contribution as well, because they can be considered as the LCE for finite perturbations.
For the investigated problem of the motion of a structure after application

of a kinetic perturbation including damping, the *reference motion* has to "converge" to the original attractor, which is the investigated stable state of equilibrium $\boldsymbol{u}_0$, see Fig. 2, at time $t \to \infty$. This means, that in the computation of the *reference motion* the kinetic perturbation has to be chosen small enough. In the case that the *perturbed motion* "converges" to $\boldsymbol{u}_0$ as well, a "stable situation" is found and $\mathcal{L}$ becomes negative. In the "unstable situation" $\mathcal{L}$ becomes either zero, when the perturbed motion converges to another stable state of equilibrium or $\mathcal{L}$ becomes positive, when the system performs an unbounded motion. Therefore within the sensitivity analysis a change of a situation from a "stable case" to an "unstable case" can be indicated by the change of the value of the LCE from some negative number either to zero or to some positive number.
For the computation of LCEs the Euclidean norm is often used, which is defined for a vector $\boldsymbol{v}^T = [v_1, v_2, \ldots, v_n]$ as

$$||\boldsymbol{v}||_{EUCL} = \sqrt{\boldsymbol{v}^T \boldsymbol{v}} = \sqrt{\sum_{i=1}^{n} v_i^2}. \tag{24}$$

Applying this norm to displacements and velocities of the perturbation vector $\tilde{\boldsymbol{u}}$ and $\dot{\tilde{\boldsymbol{u}}}$ we have to normalize the terms, in order to get a dimensionless form

$$|| \left(\tilde{\boldsymbol{u}}, \dot{\tilde{\boldsymbol{u}}} \right) ||_{EUCL} = \sqrt{\sum_{i=1}^{N_{dof}} \left(\frac{u_i^2}{L^2} + \frac{\dot{u}_i^2}{L^2 \omega^2} \right)}. \tag{25}$$

Here u_i represents the displacement for the "i"th degree of freedom and N_{dof} represents the maximum number of degrees of freedom in the problem. L represents some length and ω some eigenfrequency, which are characteristic for the considered problem. As the characteristic length L occurs in the denominator and in the numerator in equation (23), it disappears. Then only the characteristic eigenfrequency ω has to be chosen properly. A proper choice is rather difficult, because a high number of ω would underestimate the influence of the velocities on the LCE, and a low number of ω would overestimate it. Therefore it is often preferred to neglect the velocities (see e.g. Rugonyi/Bathe [17]). A further reason to neglect the velocities in the computation of LCEs in sensitivity analyses is, that the different cases – "stable" and "unstable situations" – are separated by the location of the attractors in the pre- and post-buckling regions, but not by velocities. Therefore the consideration of velocities is not significant in this analyses, moreover it may be disturbing.
A further problem to be discussed, is the phase-shift caused by application of a Newmark type scheme in solution of the equation of motion. The shift depends on the time step size Δt for the linear problem with constant matrices, whereas for nonlinear problems with variable matrices this shift depends not only on the time step size Δt but also on initial conditions $\boldsymbol{u}_0$ and $\dot{\boldsymbol{u}}_0$, see Fig. 4. Therefore the phase shifts for the "reference" and the "perturbed motions" are different, because of different kinetic perturbations leading to different initial conditions. Despite the fact that in the case of a "stable situation" both motions are directed towards the same attractor, the LCE would

get positive indicating an "unstable situation" if it is computed in each time step. This is due to the fact, that the motions converge in the amplitude, but diverge in phase. This situation can be considered as an orbital stability, but an instability according to Liapunov. To obtain the LCE correct for the problems discussed here equation (23) must be modified in a fashion, that the values are computed at certain characteristic points in time. An appropriate choice are the maximum values of the amplitude, e.g. the maximum values of the displacements.
Two different norms are proposed to compute the Liapunov Characteristic Exponent. In order to keep computing cost low, a simple norm of a selected single degree of freedom (SDOF) $\hat{u}$ is used first, where only the perturbation for that DOF is considered. In this case equation (24) can be wrote as

$$||\tilde{u}||_{EUCL} = \sqrt{\tilde{u}^2} = |\tilde{u}| = |\hat{u}_r - \hat{u}_p|. \tag{26}$$

As shown before, $\mathcal{L}$ has to be computed using the displacements at certain characteristic time points

$$\mathcal{L}_{SDOF}(t^*) = \frac{1}{t^*} \ln \frac{|\hat{u}_r(t^*) - \hat{u}_p(t^{**})|}{|\hat{u}_{r,0} - \hat{u}_{p,0}|}. \tag{27}$$

with

$$\dot{\hat{u}}_r(t^*) = \dot{\hat{u}}_p(t^{**}) = 0. \tag{28}$$

As the initial perturbation is applied by the definition of initial velocities, the denominator can not be computed at time point $t = 0$, but must be computed for $t \approx 0$ using the first maximum number of displacement $\hat{u}$ obtained for the reference motion. The advantage is, that this form excludes the velocities by the selection of the states to compute the distance $\tilde{u}$.
In general it is rather difficult to find a characteristic degree of freedom describing the motion characteristics for arbitrary loading. A more general form can be gained using the Euclidean norm of the complete perturbation vector instead of single degrees of freedom. Using equations (23) and (24) and neglecting the term with perturbation velocities $\dot{\tilde{u}}$ again we get

$$\mathcal{L}_{EUCL}(t) = \frac{1}{t} \ln \frac{\sqrt{\tilde{\boldsymbol{u}}^T(t)\tilde{\boldsymbol{u}}(t)}}{\sqrt{\tilde{\boldsymbol{u}}_0^T \tilde{\boldsymbol{u}}_0}}. \tag{29}$$

This formulation requires to store the complete displacement vector of the two considered motions at each computed time step, that may become a problem for large FE models. Further the situations "stable" and "unstable" can be separated neglecting the *direction* of the displacement vectors, as the locations of the attractors are described sufficiently by its *length*. Therefore a simplified formulation is proposed, where the norms of the displacement vectors are used instead of the norm of the perturbation vector

$$\mathcal{L}_{EUCL}(t^*) = \frac{1}{t^*} \ln \frac{\left| \sqrt{\boldsymbol{u}_r^T \boldsymbol{u}_r}\big|_{t^*} - \sqrt{\boldsymbol{u}_p^T \boldsymbol{u}_p}\big|_{t^{**}} \right|}{\left| \sqrt{\boldsymbol{u}_{r,0}^T \boldsymbol{u}_{r,0}} - \sqrt{\boldsymbol{u}_{p,0}^T \boldsymbol{u}_{p,0}} \right|}. \tag{30}$$

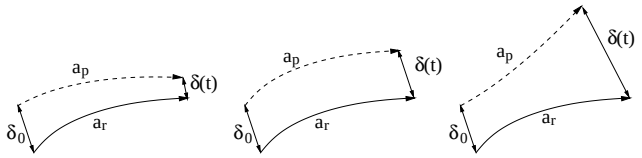

Fig. 3 Trajectories of reference and perturbed motions in phase space for the three major cases of the LCE.

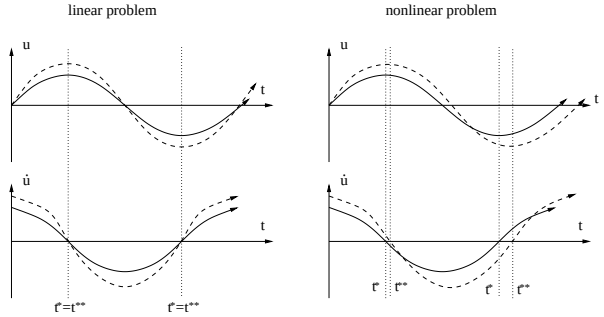

Fig. 4 Phase shift for linear and nonlinear problems caused by a Newmark type scheme.

The values at time points t^* and t^{**} denote the maximum values of the norms, thus the norms of the velocities are

$$||\dot{\tilde{\boldsymbol{u}}}_r(t^*)|| \approx ||\dot{\tilde{\boldsymbol{u}}}_p(t^{**})|| \approx 0. \tag{31}$$

This provides some legitimation to neglect the velocities in the norm.
Based on equation (18) both measures should finally converge

$$\mathcal{L} = \lim_{t^* \to \infty} \mathcal{L}_{SDOF}(t^*) = \lim_{t^* \to \infty} \mathcal{L}_{EUCL}(t^*). \tag{32}$$

Thus, $\mathcal{L}$ should be computed for $t \to \infty$ resp. for a very long time. However, numerical tests have shown, that it is sufficient to obtain convergence for the LCE with increasing time. Thus, the computation can be terminated, when the LCE has converged after a sufficiently long time span.

5 Simple examples with beam structures.

First two simple examples with beam structures – a clamped beam and a simply supported beam with elastic support – are investigated to demonstrate the sensitivity analysis procedure.

5.1 Clamped imperfect beam.

The first structure is an imperfect beam as shown in Fig. 5. It is clamped at the lower end and loaded with a vertical force $F = 1\ kN$ at the upper end.

λ represents the load multiplier. The imperfection is modeled as an angular deviation of the beam from the vertical line resp. linear horizontal distortion given by e. For the discretization 5 bilinear shell elements are used.
The load-deflection curve is shown in Fig. 6. As a characteristic coordinate the deflection w is chosen. Stable solution branches are plotted with a solid line, unstable solution branches with a dotted line. For the perfect system, i.e. $e = 0$, a symmetric stable bifurcation problem is obtained, for the imperfect system two independent solution branches exist. Using standard path following solution procedures, only the stable primary solution path can be obtained. However, given a finite perturbation at a certain load level above the bifurcation point the motion may be to the secondary solution path, if the perturbation is not to small. For small perturbations – as the equilibrium is stable – only a motion in the vicinity of the equilibrium state is obtained. In the following, a stable equilibrium state at the load level $\lambda_0 = 0.0465$ is computed first solving the corresponding non-linear equations (1). Afterwards perturbations are introduced into the system as initial velocities $\dot{\boldsymbol{u}}_0$, distributed affine to the first vibration eigenmode $\boldsymbol{\Phi}_{1,0}$ from equation (33) solved for the unloaded structure. Thus the perturbations are measured by the corresponding kinetic energy according to equation (16). For this simple example, it is obvious, that this is the critical mode.

$$\left(\boldsymbol{K}_T - \omega^2 \boldsymbol{M}\right) \boldsymbol{\Phi} = \boldsymbol{0} \tag{33}$$

In Fig. 7 the phase-portrait of the coordinate w is given for the perturbation energy $W_{kin} = 3.48\ Nmm$. Some numerical damping is introduced into the system with the Newmark parameters $\beta = 0.49$ and $\gamma = 0.9$. The two stable states of equilibrium, which are the attractors at this load level, are marked in Fig. 7 with bullets, the unstable state with a circle. Starting at the original attractor – stable state of equilibrium at $w = 18\ mm$ – with the perturbation energy $W_{kin} = 3.48\ Nmm$ the second stable state of equilibrium is just reached. For smaller energies, a vibration in the vicinity of the first state of equilibrium is obtained; for larger energies either the second or again the first state of equilibrium will be reached. In this example we have the first case mentioned in section 3: the minimum perturbation energy initiates a motion away from the stable state of equilibrium on the natural load deflection path towards another stable state of equilibrium. The sensitivity at the considered load level $\lambda_0 = 0.0465$ can then be computed using equation (17) as

$$S = \frac{1}{W_{kin,min}} = \frac{1}{3.48\ Nmm} = 0.287\ (Nmm)^{-1}. \tag{34}$$

5.2 Imperfect beam with elastic support.

The behaviour of the beam with identical geometry as discussed in previous section changes from a symmetric stable to a symmetric unstable behaviour, if it is hinged on the lower side and supported elastically on the upper side, see Fig. 8. Within the finite element model the elastic foundation is realized by an additional shell element with Young's modulus E_{sup}. Again, the displacement w is shown in the load-deflection curve in Fig. 9. The main difference to the

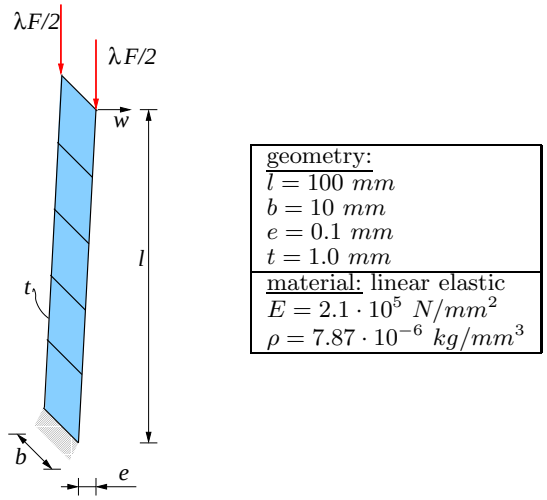

Fig. 5 Geometry and material data of the clamped imperfect beam.

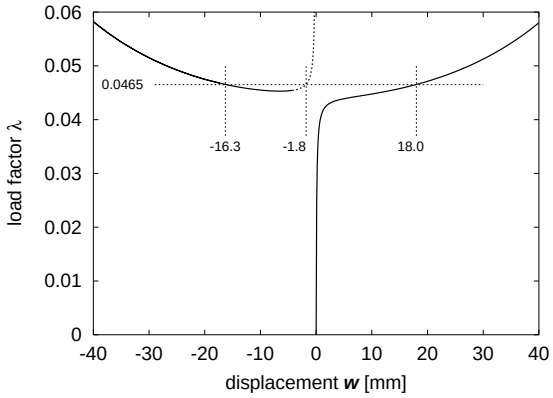

Fig. 6 Clamped imperfect beam – load-deflection curve.

clamped beam discussed in previous section is, that now no other stable state of equilibrium exists besides the stable natural equilibrium path (solid line in Fig. 9). Therefore, we have the other case mentioned in section 3: the minimum perturbation energy initiates an unbounded motion, once the structure leaves the basin of attraction of the stable state of equilibrium.
This situation is depicted in Fig. 10, where the kinetic energy $W_{kin} = 8.9\ Nm$ and $W_{kin} = 15.4\ Nm$ is introduced into the system with initial velocities $\dot{\boldsymbol{u}}_0$ distributed affine to the first vibration eigenmode. The solid line (a) in Fig. 10 for the energy of $W_{kin} = 8.9\ Nm$ shows a motion towards the stable state of equilibrium. For a larger energy $W_{kin} = 15.4\ Nm$, the dotted line (b) bypasses the unstable state of equilibrium at $w = 58.5\ mm$ leading to an unbounded motion. Thus, the energy of $W_{kin} = 15.4\ Nm$ can be taken as

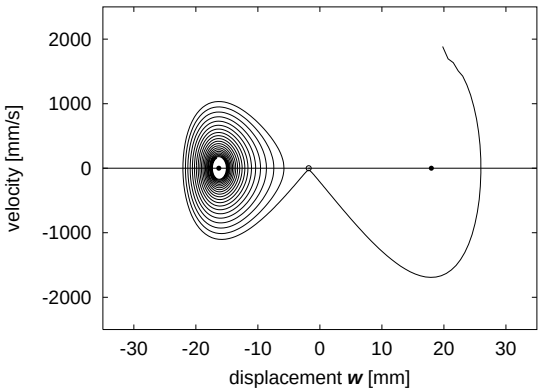

Fig. 7 Clamped imperfect beam – sensitivity; phase-portrait at $\lambda_0 = 0.0465$ for the perturbation energy $W_{kin} = 3.48\ Nmm$.

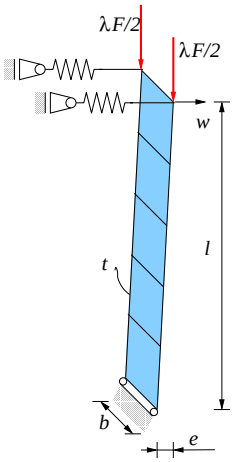

geometry:
$l = 100\ mm$
$b = 10\ mm$
$e = 1.0\ mm$
$t = 1.0\ mm$
material: linear elastic
beam:
$E = 2.1 \cdot 10^7\ N/mm^2$
support:
$E_{sup} = 1.0 \cdot 10^1\ N/mm^2$
$\rho = 7.87 \cdot 10^{-6}\ kg/mm^3$

Fig. 8 Geometry and material data of the imperfect beam with elastic support.

a measure for the sensitivity. Then, the sensitivity for the imperfect beam with elastic support at the load level of $\lambda_0 = 7$ can be given as

$$S = \frac{1}{W_{kin,min}} = \frac{1}{15.4} = 0.065\ (Nm)^{-1}. \tag{35}$$

6 Circular arch

The circular arch shown in Fig. 11 is chosen to demonstrate the application of the Liapunov Characteristic Exponents. The properties are: $E = 0.1373\ MN/mm^2$, $\nu = 0.0$, $R = 10\ m$, $t = 0.3\ m$, $\theta = 90^o$, $F = 25\ MN$, λ is the load multiplier. The arch is discretized with 18 4-node bilinear degenerated shell elements. A static analysis using the arc-length method leads

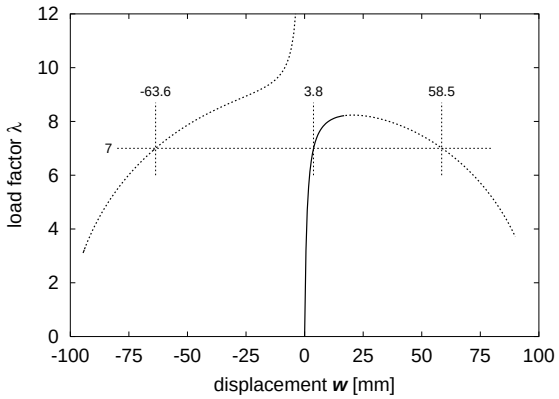

Fig. 9 Imperfect beam with elastic support – load-displacement curves and states of equilibrium at $\lambda_0 = 7$.

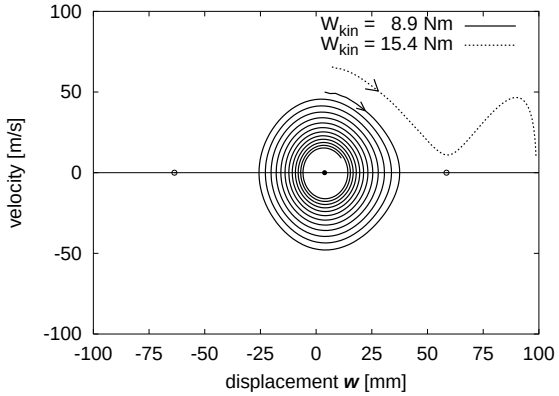

Fig. 10 Imperfect beam with elastic support – phase-portrait at $\lambda_0 = 7$

to the load deflection curve shown in Fig. 12, where the solid lines denote the stable and the dotted line the unstable equilibrium paths. The unstable paths correspond to the asymmetric shape of the arch, which will be reached by bifurcation, and the symmetric snap-through problem, which is out of interest for general practical situations with arbitrary small imperfections. In the following the sensitivity of the stable equilibrium state at the load level $\lambda_0 = 1.5$ is investigated. At this load level the structure may either reach one of the two stable states of equilibrium or one of the unstable states depicted in Fig. 12. After computing the first equilibrium state on the load curve at load level $\lambda_0 = 1.5$, the perturbation is introduced by defining the initial velocities distributed affine to the first vibration eigenmode of the unloaded structure. A reference motion is obtained for a very small perturbation energy of $W_{kin,ref} = 0.275\ MNm$; then perturbed motions for different perturbation energies of $W_{kin,per} = 2.75/16.5/22.0/27.5\ MNm$ are investigated. The LCEs are computed using equations (27) resp. (30). For the

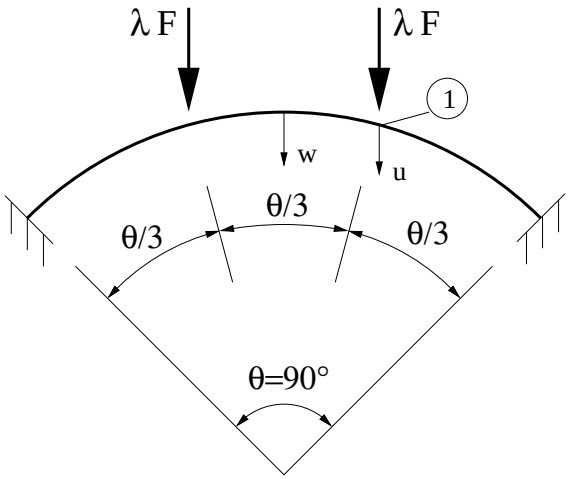

Fig. 11 Circular arch, geometry and loading.

computation of $\mathcal{L}_{_{SDOF}}$ the vertical displacement u at point 1 is used (Fig. 11). It must be noted, that a variation of the chosen dof may lead to slightly different results (see Ewert/Schweizerhof [7]). In the cases of $W_{kin,per} = 2.75$ and 16.5 MNm the structure converges to the original state of equilibrium in the pre-buckling region. As expected, both exponents, computed via the single DOF $\mathcal{L}_{SDOF}$ and via the Euclidean norm $\mathcal{L}_{_{EUCL}}$, converge to the same negative value indicating a "stable situation" (see Fig. 13 and 14), whereas the value of LCEs for the higher perturbation energies of $W_{kin,per} = 22.0$ and 27.5 MNm converge to zero indicating an "unstable situation" and a motion towards the second stable state of equilibrium in the post-buckling region. Comparing the evolution of $\mathcal{L}_{_{SDOF}}$ and $\mathcal{L}_{_{EUCL}}$ in time it is evident, that the convergence behavior is slightly different. The more general form via the Euclidean norm shows a "faster" convergence with far less oscillations and allows to judge the "stable" or "unstable situation" rather early in the analysis. This has been also confirmed by other numerical studies. Nevertheless, both formulations lead to the correct indication of the perturbed motion and can be used for this example.

7 Cylinder under axial compression

For cylindrical shell under axial compression the buckling load and the minimum post-buckling load if existent in the particular problem represent an upper resp. lower bound for the range of sensitive equilibrium states. It is obvious that at a stability point the sensitivity becomes $S = 0$, i.e. the structure buckles for infinite small perturbations. Below the post-buckling minimum load $S \to \infty$, i.e. the structures doesn't buckle for arbitrarily large perturbations. It seems to be reasonable to try to compute these "bounds" before performing the sensitivity investigations.
A further reason to investigate the singular points is the fact, that in en-

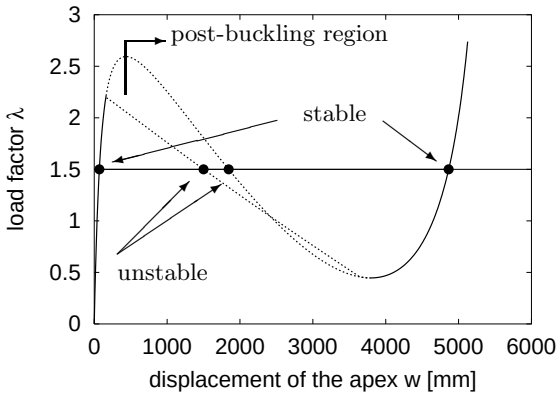

Fig. 12 Circular arch, load deflection curve for displacement "w" and states of equilibrium at load level $\lambda_0 = 1.5$.

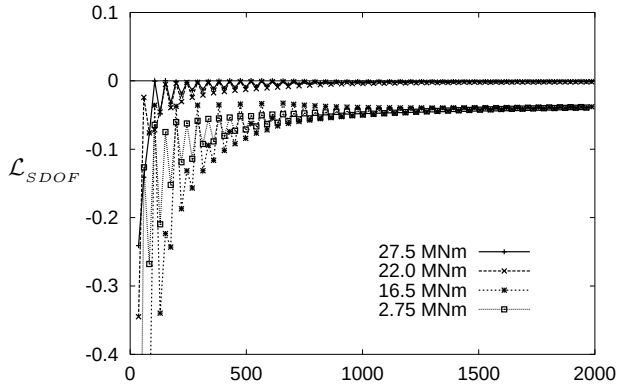

Fig. 13 Circular arch, time evolution of LCE $\mathcal{L}_{SDOF}$.

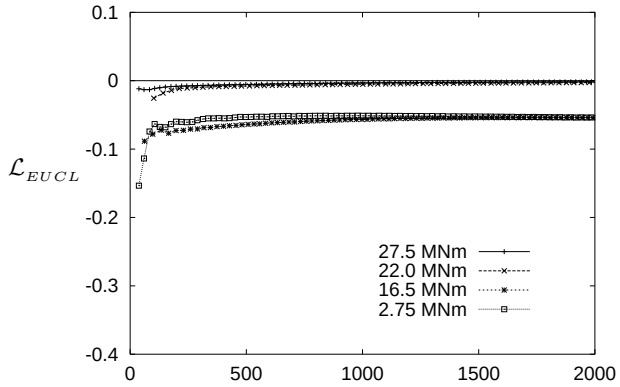

Fig. 14 Circular arch, time evolution of LCE $\mathcal{L}_{EUCL}$.

gineering practice buckling loads in combination with knock-down factors based on experiments are used in design rules. An alternative procedure proposed in design rules is based on the computation of the limit load taking into account the modification of the bifurcation load resp. the snap-through load due to geometrical imperfections. These imperfections are mostly chosen affine to the first eigenmode at the singular points. In the following first the influence of meshing including adaptive mesh refinement on the computation of stability points is investigated using low order shell elements. Afterwards a transient analysis of a cylinder under axial loading is performed, in order to obtain the complete load-deflection path with the focus on the minimum post-buckling load. Then the applicability of the two proposed versions of LCE is investigated. Finally some sensitivity investigations at various load levels are performed.

7.1 Computation of stability points using static analysis

To compute the so-called stability points criterion (5) is used in combination with the bisection procedure to take into account the geometrical nonlinear behaviour in the pre-buckling region. First of all mesh convergence studies are performed for a quarter of a perfect cylinder under axial compression using uniform mesh refinement (Fig. 15). As boundary conditions the upper and lower edges are hinged allowing displacements in axial direction. At both edges a defined load is applied in axial direction. In this case the analytical solution can be written as (see Yamaki [25])

$$\alpha = \frac{F_{cr}}{F_{cr,cl}} = 0.843 \tag{36}$$

with the normalized critical load α for the given boundary conditions and the critical load F_{cr}. The so-called classical critical load is given by

$$F_{cr,cl} = \frac{2\pi E t^2}{\sqrt{3(1-\nu^2)}}. \tag{37}$$

Two different shell elements are used in the FE model: a bilinear shell element with ANS for the transversal shear strains according to Dvorkin/Bathe [5] and a biquadratic shell element MITC9 according to Bucalem/Bathe [4]. For the implementation as nonlinear shell elements we refer to Hauptmann [8]. The results of 4 refinement steps are given in Fig. 16. The convergence diagram for the normalized buckling load α shows a much faster convergence for the biquadratic element than for bilinear elements. Even for a very fine mesh with 120x120 elements and 72240 degrees of freedom (N_{dof}) the deviation of the buckling load computed with bilinear elements from the analytical solution is still about 3% in this simple example. The reason for this is the much smoother approximation of the curved geometry using biquadratic elements. Though different eigenvectors are achieved for the starting meshes, both models converge to the same final buckling mode, see Fig. 17 and Fig. 18.
An adaptive *h*-refinement procedure might improve the convergence behaviour of a FE solution. In the present contribution a procedure partially based

on the well-known *a-posteriori* error estimator of Zienkiewicz/Zhu [26] is used. The exact error distribution $||\boldsymbol{e}||$ is defined by

$$||\boldsymbol{e}||^2 = \int_{\Omega_0} (\boldsymbol{\sigma} - \boldsymbol{\sigma}_h) : (\boldsymbol{\epsilon} - \boldsymbol{\epsilon}_h) d\Omega \tag{38}$$

with exact values of stresses $\boldsymbol{\sigma}$ resp. strains $\boldsymbol{\epsilon}$. The stresses $\boldsymbol{\sigma}_h$ resp. strains $\boldsymbol{\epsilon}_h$ are the discrete values the FE solution. As the exact values are unknown the expression (38) is approximated by

$$||\boldsymbol{e}_h||^2 = \int_{\Omega_0} (\boldsymbol{\sigma}^* - \boldsymbol{\sigma}_h) : (\boldsymbol{\epsilon}^* - \boldsymbol{\epsilon}_h) d\Omega. \tag{39}$$

The values denoted with "*" are called recovered values and are computed by a least-square fit on element patches using the so-called superconvergent patch recovery procedure (see Zienkiewicz/Zhu [26]). Using the recovered and the discrete values the error distribution can be computed and used for mesh refinement. Neumann/Schweizerhof [12] proposed to compute the discrete values using the lowest eigenvector to improve the investigations of vibration eigenmodes. In a similar fashion the values resp. the error distribution are computed here using simply the lowest eigenvector of (4) at the singular point instead of the displacement vector.
The following procedure is followed in an adaptive computation of singular points and buckling modes:

a) starting with a coarse mesh, e.g. 20x20 Elements
b) bisection to the singular point within a nonlinear computation monitoring the lowest eigenvalues of (4)
c) computation of eigenvalues and eigenmodes at the singular point, e.g. using (4)
d) computation of error distribution using the lowest eigenmode as described before
f) restart with the refined mesh with step b)

The results of an adaptive analysis using bilinear elements show, that the convergence behaviour concerning the singular point could be improved, see Fig. 19. In contrast to that the achieved buckling modes do not converge to the target mode of the uniform refined mesh, see Fig. 20. This is due to the transition elements, which appear in adaptive meshes. Such transition elements are mostly considerably distorted for curved shells compared to standard element form. Therefore they often cause artificial geometrical imperfections leading to buckling modes, which are partially totally different from the correct modes. Modeling the cylinder with biquadratic elements these imperfections introduced by imperfect geometry approximation are small enough and do not influence the computation of eigenmodes at the singular points distinctly, see Fig. 21.

7.2 Simulation of buckling behaviour as a transient process.

The advantages and disadvantages of static and transient analyses in stability investigations have been already discussed in Section 2. Due to the advantage of transient analyses the buckling behaviour of real imperfect cylinder

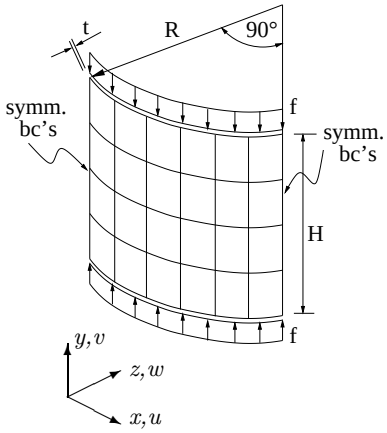

Geometry:
R = 625 mm
H = 966 mm
t = 0.56 mm

Material (steel):
E $= 2.0 \cdot 10^5\ N/mm^2$
$\nu = 0.3$

bc's for upper and lower edges:
$\boldsymbol{u} = \boldsymbol{w} = 0;\ \boldsymbol{v} \neq 0$

Fig. 15 Perfect cylinder under axial compression. Geometry, material, boundary conditions, quarter model.

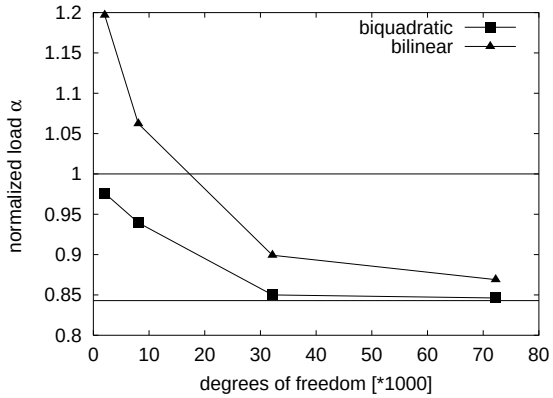

Fig. 16 Static buckling load levels (singular points) of a perfect cylinder modeled with bilinear and biquadratic elements; uniform refinement; normalized to classical critical load.

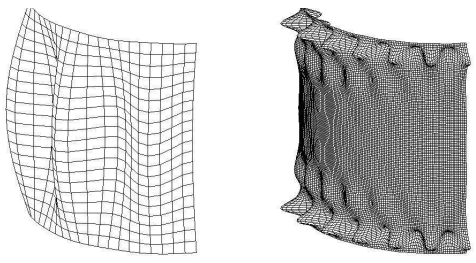

$N_{dof} = 2040$ $N_{dof} = 72240$

Fig. 17 First eigenvector at singular point for coarse and fine meshes; uniform refinement using bilinear elements.

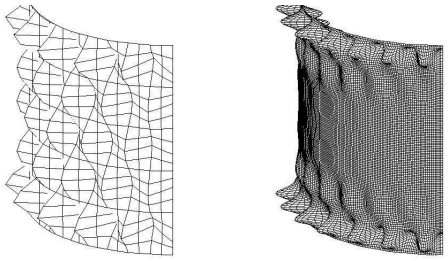

$N_{dof} = 2040$ $N_{dof} = 72240$

Fig. 18 First eigenvectors at singular points for coarse and fine meshes; uniform refinement using biquadratic elements.

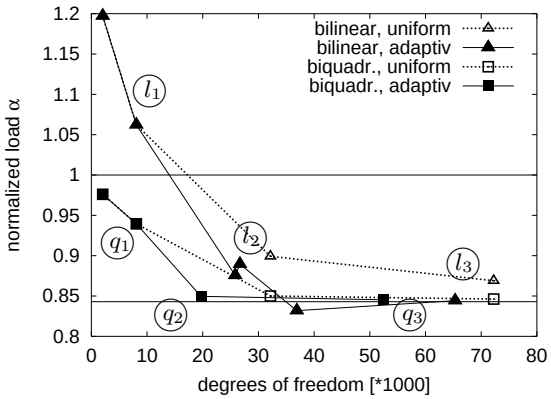

Fig. 19 Static buckling load levels (singular points) of a perfect cylinder modeled with bilinear and biquadratic elements; adaptive vs. uniform refinement.

$N_{dof} = 8080$ $N_{dof} = 25834$

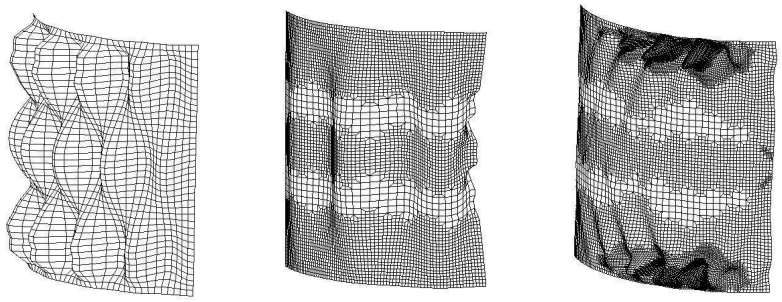

$N_{dof} = 65315$

Fig. 20 First eigenvectors at singular points for refinement steps l_1, l_2 and l_3 indicated in Fig.19; adaptive refinement using bilinear elements.

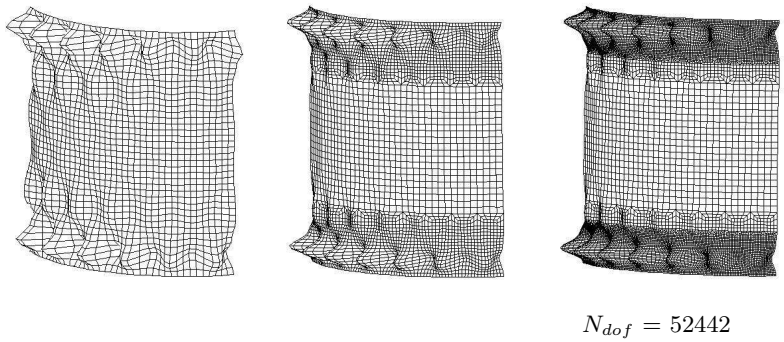

Fig. 21 First eigenvectors at singular points for refinement steps q_1, q_2 and q_3 indicated in Fig.19; adaptive refinement using biquadratic elements.

is investigated solving the equation of motion with the Newmark method. In Fig. 22 the finite element model with scaled imperfections of the investigated cylindrical shell, named AL1100, are given. The imperfection shape originates from the fabrication process and was measured at the University of Karlsruhe within the framework of a long term cooperative project, involving a series of experiments, see Knebel et al. [10]. The geometry and the material data are: $E = 2.0 \cdot 10^5\ N/mm^2$, $\nu = 0.3$, height $H = 966\ mm$, mean radius $R = 625\ mm$ and mean thickness $t = 0.56\ mm$. As boundary conditions it is assumed, that the cylinder is hinged at both edges. At the bottom edge all displacements are constrained. At the top edge displacements in axial direction are allowed. Within the FE model the loading applied by a loading plate is represented by linking the axial displacements together. Then a so-called displacement controlled loading can be applied at the upper edge resulting in an axial loading. For the transient analysis the displacements are prescribed rather closely to the real experiments with a velocity of 0.01 mm/s, i.e. very slow. The load-deflection behavior for the displacement of the top edge is given in Fig. 23. As expected, the buckling load of 165 kN is very close to the buckling load obtained from static analysis, because of the rather low loading velocity. The kinetic energy shown in the close-up view in Fig. 23 is increasing from nearly zero to approximately 3 Nm indicating the dynamic nature of the very fast buckling process. After the buckling process the post-buckling load remains nearly constant at a level of about 50 kN. This post-buckling load is very close to the load obtained in the experiment with 48 kN and also close to the value of 47.8 kN from the German design rule DIN 18800 part 4 [6]. The latter design value is computed without the reduction factor for non-elastic material behaviour. For a more detailed information about the study with transient analyses we refer to Rottner et al. [15] and [16].

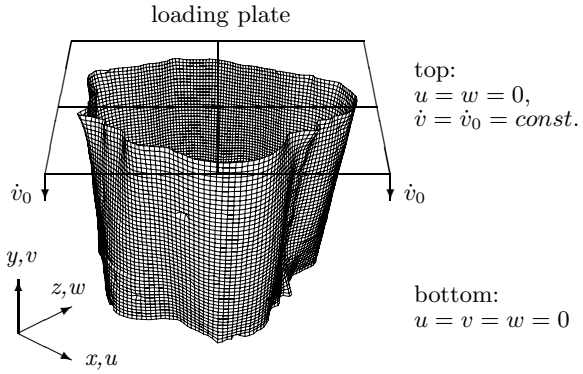

Fig. 22 System and measured geometry for axially loaded cylinder AL 1100, see Knebel et al. [10]; imperfections are scaled by a factor of 50.

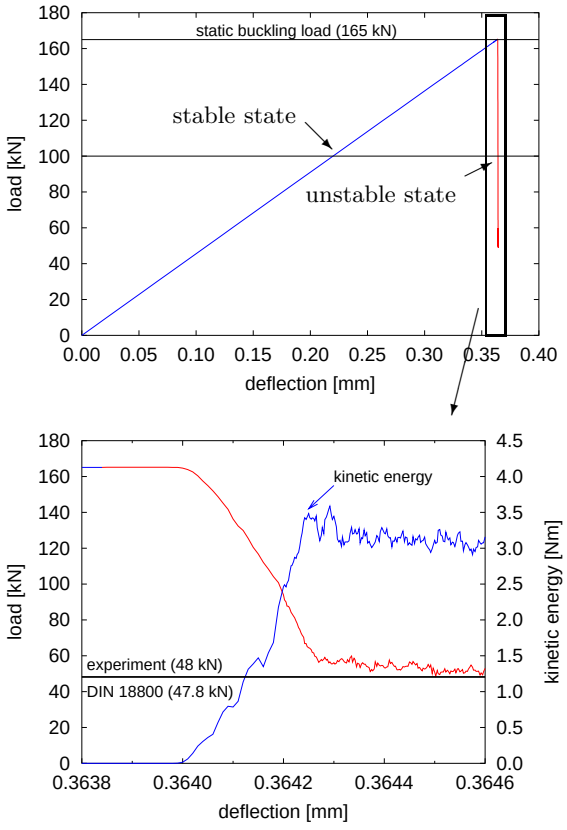

Fig. 23 Load-deflection curve for the upper boundary of the axially loaded cylinder AL 1100 and close-up of the buckling region.

7.3 Judgment of the perturbed motion.

As the cylinder shows a post-buckling load considerably below the buckling load a distinct sensitivity against perturbations can be expected in load regions between these two load levels. Due to this fact the applicability of the proposed exponents $\mathcal{L}_{SDOF}$ and $\mathcal{L}_{EUCL}$ in the sensitivity analysis of a cylinder is investigated at a load level of $F = 100\ kN$. At this load level the load deformation curve in Fig. 23 indicates, that there is at least an unstable equilibrium state besides the stable pre-buckling state. A stable equilibrium state in the post-buckling region at this load level could not be computed, as only rather small axial displacements were considered and a stable state would involve very large deformations of the cylinder after the buckling process.
In this investigation the shape of the perturbation vector is chosen affine to the first vibration eigenmode of the unloaded structure. Other shapes are discussed in the next subsection. The reference motion is obtained for a small perturbation energy of $W_{kin,ref} = 0.1\ Nm$; the perturbed motions are computed for different perturbation energies of $W_{kin,per} = 0.2/1.0/1.3/1.4\ Nm$. The displacement of the upper edge of the cylinder is chosen as characteristic dof for the LCE measures. In the final analysis with $W_{kin,per} = 1.4\ Nm$ the structure leaves the basin of attraction of the original equilibrium state after two periods and performs an unbounded motion without any further oscillations. In this particular case it was impossible to compute a sufficient number of values of the LCEs to obtain an final evolution in time to confirm the "unstable situation". However, the evolution of LCE obtained in the time interval is a clear indication, that an unbounded motion is almost guaranteed. The other considered perturbations with smaller quantities of $W_{kin,per}$ lead to a "stable situation". As also depicted in Fig. 24 and Fig. 25 the LCE results for the axially loaded cylinder can not be as easily interpreted as for the circular arch. The evolutions of $\mathcal{L}_{SDOF}$ and $\mathcal{L}_{EUCL}$ in time differ considerably; in the case of $\mathcal{L}_{SDOF}$ it is hardly possible to identify convergence for higher perturbation energies such as 1.0 Nm and 1.3 Nm. However, the more general form via the Euclidean norm converges, but rather slowly. As a consequence a very high numerical effort is needed for this confirmation.

7.4 Sensitivity analysis - variation of the perturbation vector.

As already mentioned, different perturbation shapes, i.e. shapes of the velocity distribution $\dot{\boldsymbol{u}}_0$, lead to different perturbed motions, see also [15] and [16]. An open question is, which of these shapes leads to the absolute minimum perturbation energy respectively to the maximum sensitivity? In order to answer this question for the cylinder described previously, the sensitivity is investigated at various load levels above the minimum post-buckling load of 50 kN. Four different shapes of the perturbation vector $\dot{\boldsymbol{u}}_0$ are considered. All shapes play an important role concerning the stability behavior of cylindrical shells. It is well-known that we need the least energy to initiate a vibration, if the perturbation vector is similar to the first vibration eigenmode, i.e solutions of equation (33). Therefore the first two shapes of

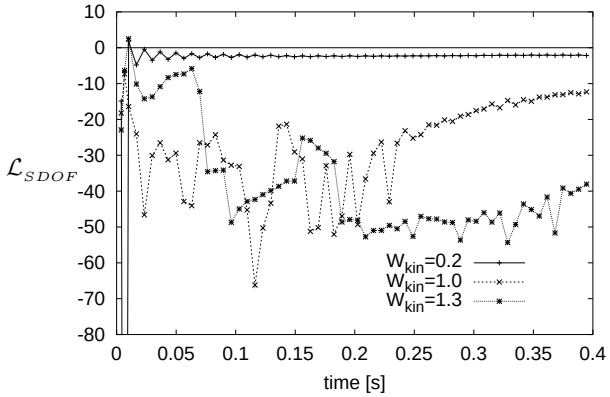

Fig. 24 Axially loaded cylinder AL1100, time evolution of the LCE $\mathcal{L}_{SDOF}$.

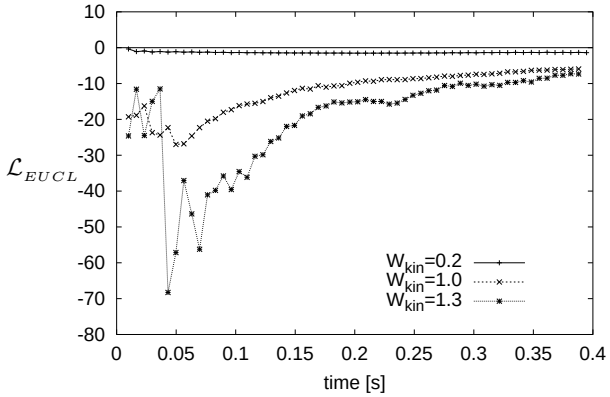

Fig. 25 Axially loaded cylinder AL1100, time evolution of the LCE $\mathcal{L}_{EUCL}$.

the perturbation vector $\boldsymbol{\Phi}_{1,load}$ and $\boldsymbol{\Phi}_{1,0}$ are first vibration eigenmodes computed for the structure at the current load level respectively for the unloaded structure. The latter chosen as pre-loading may often have little effect on the shape. As these shapes are visually almost identical for the cylinder, only one of them is depicted in Fig. 26. The third investigated shape $\boldsymbol{\Phi}_{1,S}$ is the buckling eigenmode computed at the first singular point of the tangent matrix. The fourth investigated shape $\boldsymbol{\Phi}_{buck}$ is similar to the final post-buckling shape obtained in transient analysis.

In Fig. 27 found from analyses at different load levels it becomes obvious that different perturbation shapes lead to different maximum sensitivities. At lower load levels the maximum sensitivity is obtained for $\boldsymbol{\Phi}_{buck}$. At higher load levels up to 100 kN $\boldsymbol{\Phi}_{1,load}$ resp. $\boldsymbol{\Phi}_{1,0}$ lead to the maximum sensitivity values. It must be noted, that up to this load level investigations with the vibration eigenmode $\boldsymbol{\Phi}_{\mathbf{1,0}}$ computed for the unloaded structure provide a rather good approximation for the analysis with $\boldsymbol{\Phi}_{1,load}$. At load levels above 100 kN, which are closer to the buckling load of 165 kN, the sensitiv-

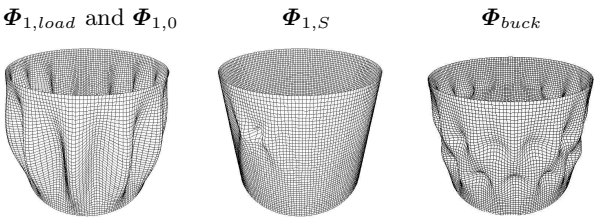

Fig. 26 Axially loaded cylinder, shapes of perturbation vector for velocity distribution.

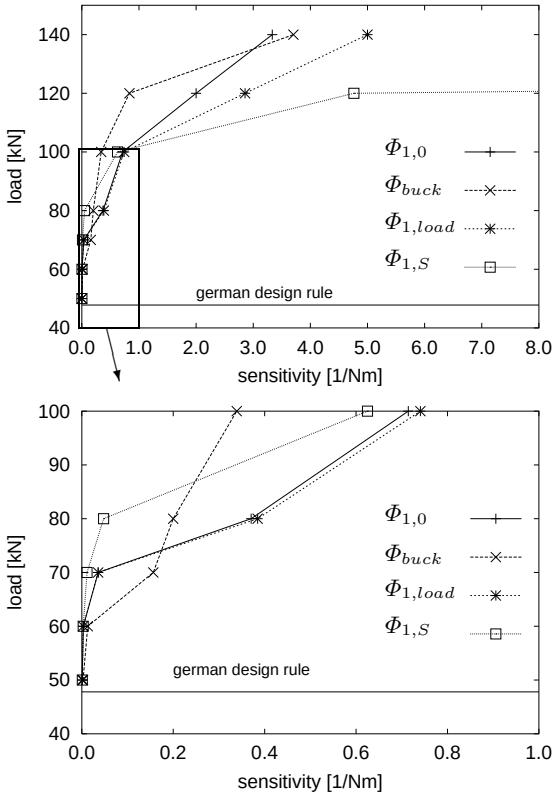

Fig. 27 Sensitivity investigations for cylinder AL 1100 under axial loading and cut-out between 0.0 and 1.0; variations of perturbation shape.

ity against $\boldsymbol{\Phi}_{1,S}$ is much higher than against the other investigated shapes. Below the load level of 50 kN, which is the minimum post-buckling load, no sensitivity was found, even for perturbation energies much larger than the internal energy at the buckling point. The close-up in Fig. 27 shows that up to 60 kN almost no difference in the sensitivity is visible and that up to 70 kN the sensitivity is rather small.

8 Cylinder under external pressure loading

8.1 Buckling behaviour

Compared to the cylinder under axial loading, where the loading can be either modeled by a force or by a displacement driven control, pressure loading on a cylinder cannot be modeled by prescribed displacements, because the load is applied to the total surface of the cylinder. The only possibility to determine a minimum post-buckling load for the pressure load is by variation of the history of the loading process. For this reason a loading-holding-unloading process providing an internal vacuum loading was chosen modeled by a closed cylinder and an associated piston. The piston can be moved creating vacuum with a controlled volume, see Fig. 28. The geometry and material data of the cylinder are identical to the cylinder under axial loading described previously. All displacements of the lower edge are constrained, whereas at the top edge only the vertical displacements are admitted.
As the loading process in the simulation is rather fast with $v_P = 1.0\ m/s$ the cylinder starts to buckle in the loading phase at a fairly high value of approximately $0.005\ N/mm^2$, the so-called dynamic buckling load, compared to the static buckling load, see Fig. 30. Then in the holding phase the value for the vacuum is decreasing, due to the volume reduction of the cylinder, as a result of the buckling process. Herein the volume reduction dV is defined as

$$dV = \frac{V_{cyl,0} - V_{cyl,1}}{V_{cyl,0}} \cdot 100\%. \tag{40}$$

The buckling pattern is strongly changing showing mode jumping within the holding process. However, the reduction of vacuum thus the volume change in the holding phase is rather small compared to the post-buckling load observed for the axially loaded cylinder. In the unloading phase a completely different equilibrium path compared to the loading process is followed for both unloading velocities shown. Finally the cylinder "snaps" back into the undeformed configuration at a load level of approx. $0.0023\ N/mm^2$, which is significantly lower than both the static and the dynamic buckling load. This load value could be considered as the minimum post-buckling load for the pressure loading modeled by vacuum and it is close to the value found in the German design rule [6]. We also have to point out, that the load-deformation path is also varying with varying unloading velocities. As expected, in cases of lower velocities the minimum post-buckling load is closer to the value found in the German design rule, see Fig. 30 .

8.2 Sensitivity analysis for the cylinder under external pressure.

The sensitivity studies for the cylinder under external pressure have been performed in a similar fashion as for the axially loaded cylinder. First a static analysis is performed up to the considered load level. After this a transient analysis follows with an applied perturbation using the vibration eigenmode $\boldsymbol{\Phi}_{1,0}$. As the pressure loading has to remain constant for this investigation

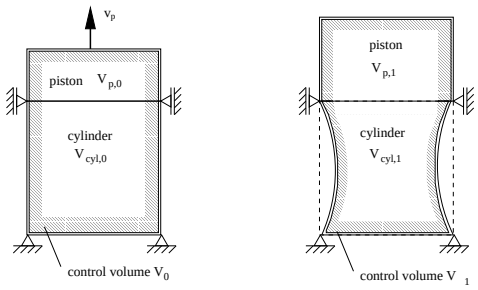

Fig. 28 Cylinder under vacuum loading, loading by piston motion; initial state and situation after buckling.

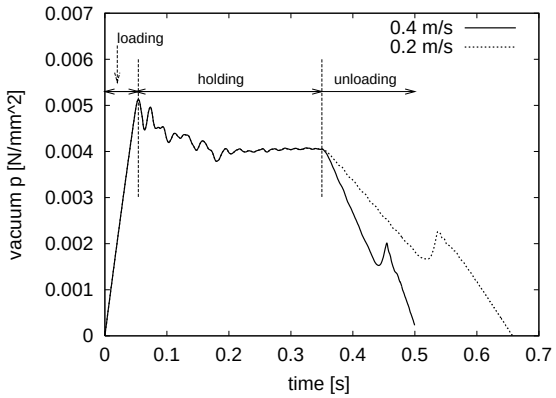

Fig. 29 Vacuum vs. time for cylinder under vacuum loading with two different unloading velocities.

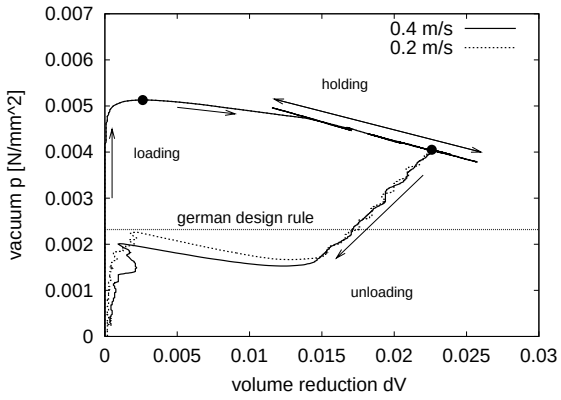

Fig. 30 Vacuum vs. volume reduction for cylinder under vacuum loading with two different unloading velocities.

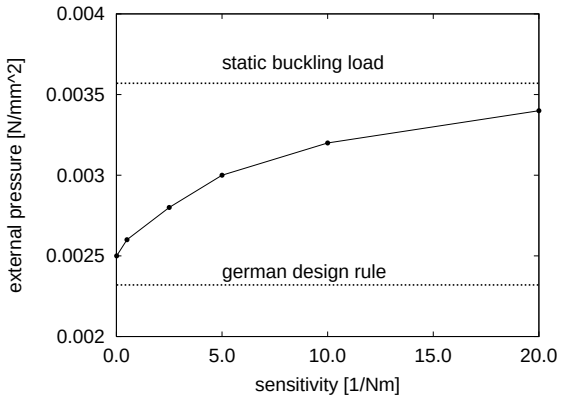

Fig. 31 Sensitivity diagram for cylinder AL 1100 under external pressure.

not a vacuum loading, but an external pressure loading is modeled here. As expected, no sensitivity is found below the load level of 0.0025 N/mm^2 which is close to the post-buckling load level obtained in the previous section, see Fig. 31. In the vicinity of the static buckling load of 0.00357 N/mm^2 the sensitivity becomes rather large, similar as for axial loading.

9 Aspects for the stability design of shells.

Sensitivity can be used for design purposes by checking the real quantity of the necessary perturbation energy and judging the vulnerability of the design. The sensitivity studies may even lead to an increase of the design load level compared to current rather conservative design rules for load regions with very low sensitivity.
In Fig. 32 the sensitivity values are shown for the cases of axial and external pressure loading. The load is normalized with respect to the static buckling load of 165 kN for the axial loading and 0.00357 N/mm^2 for the external pressure loading. Comparing both curves we can conclude, that for the case of axial loading the sensitive region is much larger than for the case of external pressure. However, the sensitivity values are rather low at lower load levels for the axial loading. Therefore it seems to be reasonable to propose an increase of the design load level for the axial loading case, e.g. up to 0.5 of the static buckling load. For the external pressure the sensitivity is quickly increasing beyond a load level of 0.7. Thus, for external pressure an increase of the design pressure value beyond the completely insensitive region cannot be suggested. The application of some sensitivity studies may assist in the modernization of current overly conservative design rules.

10 Conclusions

The investigations on the buckling of cylindrical shells taking transient analysis into account show that a better judgment of the stability of a current

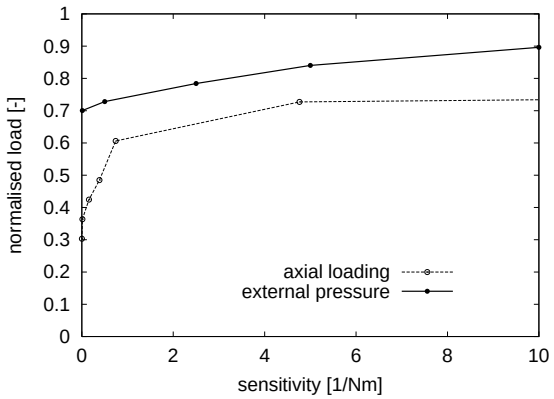

Fig. 32 Sensitivity for the cylinder AL 1100 for axial and external pressure loading. Load normalized to static buckling load obtained by eigenvalue analysis.

pre-buckling situation is possible than with any static analysis. In the case of vacuum loading the post-buckling studies had to be performed by considering a loading-holding-unloading process. The sensitivity studies allow a good judgment of the current stable equilibrium state in the pre-buckling region concerning the "practical" stability of these states for both considered load cases. In particular, valuable information can be gained for practical design purposes.

References

1. S. Baguet, B. Cochelin (2000) Direct computation of paths of limit points using the asymptotic numerical method. in M. Papadrakakis, ed., Forth International Colloquium on Computation of Shell & Spatial Structures IASS-IACM, Chania.
2. G. Benettin, L. Galgani and J.M. Strelcyn (1976) Kolmogorov entropy and numerical experiments. Phys. Rev. Vol: 14, 2338-2345.
3. B. Brendel (1979) Geometrisch nichtlineare Elastostabilität. Dissertation, Institut für Baustatik, University Stuttgart. In German.
4. E. N. Bucalem, K. J. Bathe (1993) Higher-order MITC general shell elements. Int. J. Num. Meth. Eng., Vol: 36. 3729 – 3754.
5. E. N. Dvorkin, K. J. Bathe (1989) A continuum mechanics based four node shell element for general nonlinear analysis. Eng. Comp., Vol: 1, 77 – 88.
6. DIN 18800, Teil 4 (1990) Stahlbauten, Stabilitätsfälle, Schalenbeulen, Normenausschuss Bauwesen, Deutsches Institut für Normung e.V., Beuth Verlag GmbH, Berlin. In German.
7. E. Ewert, K. Schweizerhof (2003) On sensitivity investigations of thin-walled shell structures using transient finite element analysis and finite perturbations. PAMM Vol: 3, 170–171.
8. R. Hauptmann (1997) Strukturangepaßte geometrisch nichtlineare Finite Elemente für Flächentragwerke. Dissertation. Institut für Mechanik, University Karlsruhe. In German.
9. P. Helnwein (1996) Zur initialen Abschätzbarkeit von Stabilitätsgrenzen auf nichtlinearen Last-Verschiebungspfaden elastischer Strukturen mittels der Methode der Finiten Elemente. Dissertation, University Vienna. In German.
10. K. Knebel, U. Peil, U. Schulz, K. Schweizerhof and T. Ummenhofer(2000) Stabilität von stählernen Silozylinderschalen bei Belastung mit ruhendem und

bewegtem Schüttgut, in Eibl, J. and Gudehus, G., eds. DFG Reihe Sonderforschungsbereiche, SFB 219 Silobauwerke und ihre spezifischen Beanspruchungen, Wiley-VCH, Weinheim, Germany. In German.
11. B. Krplin, D. Dinkler, J. Hillmann (1984) An energy perturbation applied to nonlinear structural analysis. Com. Meth. Appl. Mech. Eng., Vol:52, 885 – 897.
12. J. Neumann and K. Schweizerhof (2003) Adaptive FE Diskretisierung zur Bestimmung der Eigenfrequenzen von Flächentragwerken. PAMM, Vol: 2, 246-247. In German.
13. E. Ramm (1976) Geometrisch nichtlineare Elastostatik und Finite Elemente. Habilitationsschrift. University of Stuttgart. In German.
14. E. Riks, C.C Rankin and F.A. Brogan (1996) On the solution mode jumping phenomena in thin-walled shell structures. Comp. Meth. Appl. Mech. Eng. Vol:136, 59-92.
15. T. Rottner, P. Vielsack, K. Schweizerhof (2000) Transient analysis to compute post-buckling solutions for axially loaded cylindrical shells and sensitivity investigations, in M. Papadrakakis, ed., Forth International Colloquium on Computation of Shell & Spatial Structures IASS-IACM, Chania.
16. T. Rottner (2000) Sensitivitätsanalyse stabiler Gleichgewichtslagen dünnwandiger Strukturen unter Verwendung von Lösungsverfahren für Parallellrechner. Dissertation, Institut für Mechanik, University Karlsruhe. In German.
17. S. Rugonyi, K. J. Bathe (2001) Lyapunov characteristic exponent calculation for finite element discretized models. Proceedings: First MIT Conference on Computational Fluid and Solid Mechanics, 1640-1643.
18. K. Schweizerhof, R. Hauptmann, K. Knebel, M. Raabe and T. Rottner (1998) Statische und dynamische FE-Stabilitätsuntersuchungen an Siloschalen mit ungleichförmiger Schüttgutfüllung. Finite Elemente in der Baupraxis. Wriggers, P., Meissner, U., Stein, E. and Wunderlich, W. Ernst & Sohn Verlag, 287-306. In German.
19. K. Schweizerhof, P. Vielsack, T. Rottner, and E. Ewert (2002) Stability and Sensitivity Investigations of Thin-Walled Shell Structures Using Transient Finite Element Analysis. WCCM V, Vienna.
20. I. Spohr (1998) Störenergie-Konzept für den elasto-plastischen Beulsicherheitsnachweis beliebig belasteter Schalen. Dissertation, Istitut für Statik, University Braunschweig. In German.
21. G. Tranel (1994) Stabilitätsnachweis beliebiger Schalen mit dem Konzept der Störenergie. Dissertation, Istitut für Statik, University Braunschweig. In German.
22. P. Wriggers, W. Wagner, C. Miehe (1988) A quadratically convergent procedure for the calculation of stability points in finite element analysis, Comp. Meth. Appl. Mech. Eng. Vol:70, 329-347.
23. W. Wagner, P. Wriggers (1988) A simple method for the calculation of postcritical branches. Engineering Computations, Vol: 5, 103-109.
24. P. Vielsack, W. Sprenger, T. Hesse (1995) Sensitivität stabiler Gleichgewichtszustände elastischer Strukturen. Stahlbau Vol: 64, 321-325. In German.
25. N.Yamaki (1984) Elastic stability of circular cylindrical shells. North-Holland series in applied mathematics and mechanics, Vol: 27.
26. O. Zienkiewicz and J. Zhu (1992) The superconvergent patch recovery and a posteriori error estimates. Part 1: The recovery technique. Part 2: Error estimates and adaptivity. Int. J. Num. Met. Eng., Vol: 33, 1131–1382.